Morphology of Thin Films of Diblock Copolymers on Surfaces Micropatterned with Regions of Different Interfacial Energy

Richard D. Peters, Xiao M. Yang,† and Paul F. Nealey*

Department of Chemical Engineering and Center for Nanotechnology, University of Wisconsin, Madison, Wisconsin 53706

Received June 11, 2001; Revised Manuscript Received November 19, 2001

ABSTRACT: Self-assembled (SA) films of octadecyltrichlorosilane were patterned by exposure to X-rays in air through a mask to produce chemically patterned surfaces. The irradiated regions of the SA films underwent surface chemical modification from nonpolar, hydrophobic surfaces to polar, hydrophilic surfaces. The degree of chemical modification increased with increasing exposure dose. The behavior of thin films of symmetric poly(styrene-*b*-methyl methacrylate) (P(S-*b*-MMA)) was investigated on the chemically patterned surfaces exposed to X-rays at doses ranging from 800 to 2000 mJ/cm^2. P(S-*b*-MMA) films exhibited symmetric, neutral, and asymmetric wetting on these surfaces with increasing dose. The area and height of islands and holes that formed on the free surface of the films depended on the interfacial energy between the film and the surface. If the difference in interfacial energies ($\Delta\gamma$) between the surface and both PS and PMMA was small, islands or holes formed that had a smaller average area and smaller step height than islands or holes that formed on surfaces where $\Delta\gamma$ was large. Additionally, perpendicular lamellae were detected at the edge of islands when $\Delta\gamma$ was small but were not detected at the edge of islands when $\Delta\gamma$ was large. The island/hole morphologies observed over regions where $\Delta\gamma$ was small were concluded to be the result of slow rates of formation and growth of the topography. Films of initial thickness from 1.75 to 2.75L_o, where L_o is the bulk lamellar period, were studied on chemically patterned surfaces where both exposed and unexposed regions had large values of $\Delta\gamma$. On these surfaces, regions of the film were observed to remain flat and featureless even when the film thickness did not equal a quantized value of the thickness. These flat regions were concluded to be due to either mass transport of excess material from island-forming regions across the pattern boundaries to regions with deficits (hole-forming regions) or deformation of lamellae in the outer layer of the block copolymer film. On surfaces with large values of $\Delta\gamma$, ordering was fast and allowed large-scale cooperation between adjacent regions of the polymer film to set up the film morphology during the very early stages of annealing.

Introduction

Block copolymers are interesting materials for nanofabrication because they spontaneously form ordered, periodic structures with dimensions between 10 and 100 nm.[1,2] The size and shape of the nanostructures can be controlled easily by manipulating the molecular mass, *M*, and composition of the copolymer. Thin films of block copolymers have been investigated for the fabrication of nanowires,[3,4] magnetic storage media,[3] quantum dot arrays,[5−8] and photonic crystals.[9−11] In all cases, it is desirable to control the ordering and orientation of the nanostructures over macroscopic dimensions. The morphology of the thin films is determined by a minimization of surface and interfacial energies (block−block interactions and block−substrate interactions) while trying to maintain the bulk lamellar period, L_o. In this paper, the effects of varying interfacial energies between the blocks of a symmetric diblock copolymer and a chemically patterned substrate on the ordering of lamellae and morphology of surface relief structures is investigated.

On chemically homogeneous surfaces, differences in interfacial energy between the surface and the blocks of the copolymer generally induce the lamellar domains to orient parallel to the plane of the film to minimize the free energy. For unconfined thin films of symmetric diblock copolymers, the parallel orientation of the lamellae results in a quantization of the total film thickness. Film thickness is quantized to values of nL_o for symmetric wetting when the same block wets both interfaces or $(n + {}^1/_2)L_o$ for asymmetric wetting when different blocks wet the two interfaces, where n is an integer. For films with thicknesses (t) not equal to these quantized values (t_n), islands or holes with step heights equal to L_o form on the free surface of the films.[12−15] Mayes et al. investigated the ordering process of thin films of symmetric poly(styrene-*b*-methyl methacrylate) (P(S-*b*-MMA)) with increasing annealing time.[16] They found that ordering begins at the substrate with lamellae oriented parallel to the plane of the film due to preferential wetting of one of the blocks and propagates through the thickness of the film toward the free surface. They hypothesized that during the ordering process the lamellar layers are perforated with channels that allow molecules to move between layers and allow the ordering process to proceed to completion.

We[17] and others[18−20] have studied previously the effects of interfacial energy on the wetting behavior of thin films of symmetric diblock copolymers on homogeneous surfaces. Substrates with tunable interfacial energies with P(S-*b*-MMA) have been fabricated using surface-grafted random copolymers with varying composition[18−20] and using self-assembled (SA) films of alkylsiloxanes exposed to different doses of X-rays in air.[17,21] In both types of experiments, symmetric, neutral, and asymmetric wetting were observed as the interfacial energy between the surfaces and the polymer film were varied. In our previous experiments, we used the initial film thickness, the measured value of L_o, and

* Corresponding author. E-mail: nealey@engr.wisc.edu.
† Current address: Seagate Research Center, River Park Commons, Suite 550, 2403 Sidney St., Pittsburgh, PA 15203-2116.

10.1021/ma011003e CCC: $22.00
Published on Web 01/26/2002

the type of topography that forms to determine the wetting behavior of the copolymer films.[17,22]

Thin films of diblock copolymers on chemically micropatterned surfaces (alternating regions of different surface chemistry, i.e., alternating regions of different interfacial energy) have been studied to examine topography,[23−27] pattern replication,[23−25] polymer wetting,[23,28] and mass transport across pattern boundaries[25−27] in the copolymer films. Variations in interfacial energy within a given region or between adjacent regions have not been explored. In this paper, surfaces are patterned with alternating regions of different wetting behavior: symmetric wetting/weakly symmetric wetting, symmetric wetting/neutral wetting, symmetric wetting/weakly asymmetric wetting, and symmetric wetting/asymmetric wetting. On areas of the polymer films over weakly symmetric or weakly asymmetric wetting regions, topography is smaller with shorter step heights than on areas of the polymer film over symmetric or asymmetric wetting regions after annealing for 24 h. This difference in topography is related to the rates of formation and growth of topography due to the presence of defects in the lamellar structure. For symmetric wetting/asymmetric wetting patterns, cooperation between regions of the polymer film over the different wetting regions results in film surfaces that are smooth when $t \neq t_n$.

Experimental Section

Materials. Polished test grade silicon ⟨100⟩ wafers were purchased from Tygh Silicon. Octadecyltrichlorosilane (OTS, $CH_3(CH_2)_{17}SiCl_3$, 95%) was purchased from Gelest and was used as received. Symmetric poly(styrene-*b*-methyl methacrylate) was purchased from Polymer Source, Inc. The number-average molecular mass (M_n) was 51 200 g/mol, the polydispersity was 1.06, the styrene volume fraction was 0.48, and L_o was 30 nm. Toluene (99.8%, anhydrous), chloroform (99+%, anhydrous), and poly(acrylic acid) (25 wt % solution in water) were purchased from Aldrich and were used without further purification. Ethanol (dehydrated, 200 proof) was purchased from Aaper Alcohol and Chemical Co. and was used as received. Ruthenium tetroxide (0.5% aqueous solution) was purchased from Polysciences, Inc.

Deposition of Self-Assembled Films. Silicon wafers were cleaved into pieces approximately 2 cm × 2 cm, and were cleaned by immersion in a piranha solution (7/3 (v/v) of 98% H_2SO_4/30% H_2O_2) at 90 °C for 30 min. The silicon pieces were immediately rinsed with deionized water (resistivity ≥ 18 MΩ·cm) several times and were blown dry with nitrogen. The clean substrates were immersed in a 0.1% (v/v) solution of OTS in toluene in a glovebox with a nitrogen atmosphere. The substrates were removed from the silane solution after 24−48 h. After the substrates were removed from the silane solution, they were rinsed with chloroform for approximately 30 s, and excess chloroform was allowed to evaporate. The films were rinsed with absolute ethanol and were dried under a stream of nitrogen. Thin films of P(S-*b*-MMA) exhibited symmetric wetting on the SA films after annealing at 180 °C for 24 h.[22]

Patterning of SA Films with X-rays. SA films of OTS were patterned by exposure to soft X-rays through a mask in the ES-1 beamline at the Center for Nanotechnology (CNT). CNT facilities are located at the Synchrotron Radiation Center at the University of Wisconsin−Madison. The wavelength (λ) of the broadband radiation was centered at 1.1 nm with $\lambda/\Delta\lambda \approx 3$. The intensity of the incident radiation was 17 to 38 mW/cm^2 and varied with the synchrotron ring current. Samples were irradiated at an incident angle of 90°. Nickel transmission electron microscopy (TEM) grids (300 mesh) were used as masks, and the grids had square-shaped openings approximately 50 μm × 50 μm with 30 μm grid bars (see Figure 1). The grids were held in contact with OTS-covered substrates by magnets placed behind the substrates. The exposures were carried out in a chamber with a pressure of 1 Torr of air. The intensity of the X-ray beam was attenuated when passing through the atmosphere of the chamber. The reported doses from 800 to 2000 mJ/cm^2 refer to the dose that is delivered to the chamber. The effective dose that reaches the surface of the SA films was approximately 93% of the reported dose.[21]

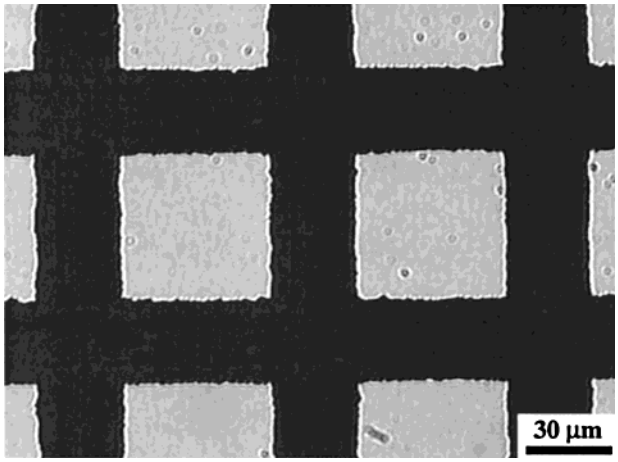

Figure 1. Transmission optical micrograph of 300-mesh nickel TEM grid showing the dimensions of the mask.

Sample Preparation. Thin films of P(S-*b*-MMA) were deposited onto patterned OTS-covered SiO_x/Si substrates by spin coating from a dilute solution (2% w/w) of the copolymer in toluene. The thickness of the polymer films was varied by changing the spin coating rate from 1800 to 4000 rpm. The initial thicknesses of the films were determined by scraping some of the polymer away from the surface with a razor blade and by measuring the difference in height between the substrate and the surface of the film using an Alpha Step 200 profilometer (0.5 nm resolution). The uncertainty of the thickness measurements was 2 nm. The polymer films were annealed at 180 °C in a vacuum oven for 24 h. After annealing, the morphology of the films was investigated using optical microscopy, atomic force microscopy (AFM), and TEM.

Optical Microscopy. Films were imaged using an Olympus model BX600 optical microscope in reflection mode. Island and hole topography resulted in contrast (different interference colors) due to differences in film thickness. Holes appear as lighter areas, and islands appear as darker areas in the optical micrographs.

Atomic Force Microscopy. The surface topography of the polymer films was imaged using a Nanoscope III MultiMode AFM from Digital Instruments in contact mode. A triangular cantilever with an integral pyramidal Si_3N_4 tip was used. The typical imaging force was on the order of 10^{-9} N.

Lateral Force Microscopy. Lateral force microscopy (LFM) of the surfaces of some of the films was performed under similar conditions as AFM with the Nanoscope III MultiMode AFM. A similar Si_3N_4 tip was used with a scan angle of 90°.

Transmission Electron Microscopy. The internal structure of the films was studied using a JEOL 200CX transmission electron microscope at 200 kV in the bright field mode. Samples were imaged in plane-view. A layer of carbon (ca. 20 nm thick) was evaporated onto the surface of films and then covered with a 25% aqueous solution of poly(acrylic acid) (PAA). After the sample was dried in air overnight, the P(S-*b*-MMA)−carbon−PAA composite was peeled off the substrate and floated on deionized water with the PAA side down. After the PAA layer dissolved, the floating film was collected onto TEM grids. The films were then exposed to the vapor of the RuO_4 solution for 15 min. The RuO_4 selectively stains the PS block and provides contrast in electron density.

Results and Discussion

Wetting Behavior of P(S-*b*-MMA) as a Function of Interfacial Energy. The wetting behavior of thin

films of P(S-*b*-MMA) was previously studied as a function of interfacial energy on self-assembled monolayers (SAMs) of OTS exposed to X-rays in air with increasing dose.[17] With increasing dose, the conversion of surface methyl groups on SAMs of OTS to polar aldehyde and hydroxyl groups increases.[21] The block that preferentially wets the substrate was shown to be the block having a lower interfacial energy (γ) with the exposed OTS. For doses between 300 and 1000 mJ/cm^2, $\Delta\gamma = \gamma_{PMMA/OTS} - \gamma_{PS/OTS} > 0.1$ mJ/m,[29,30] and the polymer films on these surfaces exhibited symmetric wetting with the PS block preferentially wetting the substrate. At a dose of 1200 mJ/cm^2, $\Delta\gamma = 0$ mJ/m^2, and the polymer films on these surfaces exhibited neutral wetting with both blocks wetting the substrate. This dose that results in neutral wetting of the P(S-*b*-MMA) films is referred to as the neutral dose. For doses of 1600 mJ/cm^2 or higher, $\Delta\gamma < -2$ mJ/m^2, and the polymer films on these surfaces exhibited asymmetric wetting with the PMMA block preferentially wetting the substrate. For doses near the neutral dose such that $|\Delta\gamma|$ is very small, the surfaces are weakly preferential to one block of the copolymer. For these surfaces, the wetting behavior is referred to as "weakly symmetric" for doses slightly less than the neutral dose and "weakly asymmetric" for doses slightly greater than the neutral dose. As shown later in this paper, the neutral dose was approximately 1000 mJ/cm^2 on the SA films of OTS used for the experiments presented in this paper compared to a neutral dose of 1200 mJ/cm^2 on SAMs of OTS used in previous experiments.[17] The slightly different values for the neutral dose were due to structural differences due to different deposition conditions between SA films and SAMs of OTS.[22]

Patterning SA Films of OTS. The pattern dimensions and shapes of the block copolymer films shown in the figures of this paper do not match perfectly with the pattern of the grid mask shown in Figure 1. The patterns in the copolymer films generally have rounded corners and larger exposed regions compared to the mask. The low fidelity between the mask and the patterns in the polymer films may be due to: (1) lateral spreading of primary and secondary electrons emitted from the substrate, (2) gaps between the mask and the substrate, or (3) charging of the mask. (1) The chemical modification of the OTS films depends on primary and secondary electrons that are emitted from the substrate upon irradiation with X-rays.[21] These electrons produce free radicals at the surface of the OTS film that react with oxygen to form hydroperoxy radicals. These hydroperoxy radicals decompose to aldehyde and hydroxyl groups. Some of the electrons generated by interactions of photons with the substrate in exposed regions may have had sufficient energy and appropriate trajectories to effect chemical modification of the OTS in unexposed regions. The number of electrons emitted from the silicon substrate that affected the unexposed regions decreased with distance from the interface between exposed and unexposed material. (2) Gaps between the Ni grids and the substrate may have been on the order of tens of μm and may have produced diffraction effects. (3) Interactions between incident photons and the Ni mask may have produced charging effects that altered the flight path of electrons from the substrate or produced discharge plasmas. The mask was isolated and became positively charged as electrons were emitted from the mask during irradiation. In this paper, the patterned surfaces are described as existing of exposed, unexposed, and transition regions. Exposed regions refer to areas of the OTS films where chemical modification occurred that are directly irradiated with X-rays, unexposed regions refer to areas that were not irradiated with X-rays and where chemical modification did not occur, and transition regions refer to areas between exposed and unexposed regions where chemical modification may have occurred due to scattering of primary and secondary electrons, diffraction effects, or charging effects. Square regions of the films are exposed, grid regions of the films are unexposed, and areas between these two regions at the pattern boundaries are the transition regions. The width of the transition region varies from sample to sample and cannot be predicted. Transition regions were not observed previously on samples patterned using standard membrane-type X-ray masks[23,28] or maskless interferometric patterning with extreme ultraviolet radiation.[31]

Symmetric Wetting/Weakly Symmetric Wetting Patterns: Size of Island Topography Dependent on Interfacial Energy. Figure 2 shows two optical micrographs of thin films of P(S-*b*-MMA) deposited and annealed on patterned OTS exposed to X-rays at doses of 800 and 900 mJ/cm^2. For SA films of OTS, these doses are slightly less than the neutral dose for films of P(S-*b*-MMA). An AFM image and cross-sectional profile of the film depicted in Figure 2b is shown in Figure 2c. For exposure doses of 800 and 900 mJ/cm^2, islands formed over both exposed and unexposed regions indicative of symmetric wetting over both regions for the initial film thickness of $2.2L_o$ (66 nm). The average area of the islands over the exposed regions (1.5 and 1.9 μm^2 for Figure 2, parts a and b, respectively) was smaller than the average area over unexposed regions (5.7 and 3.9 μm^2 for Figure 2, parts a and b, respectively). From the AFM cross-sectional profile, the step height of the islands at the edge of the pattern boundary on the unexposed side equaled 30 nm (L_o) as expected for island formation for a symmetric wetting block copolymer, but near the center of the exposed region, the step height of the islands was ~13 nm, less than L_o. This value is approximately $^1/_2L_o$, but to our understanding this value has no physical significance and is arbitrarily less than L_o depending upon the annealing time for the film. From the cross-sectional profile, the height difference between exposed and unexposed areas was ~0 nm; the islands over both exposed and unexposed regions are on the same plane of the film.

Several groups have studied the kinetics of the formation and growth of islands and holes on thin films of symmetric diblock copolymers.[14,32−35] The formation stage of the surface relief structures is correlated with the lamellar ordering process; individual domains are formed during this stage, and their height increases up to L_o with increased ordering of the parallel lamellar structure.[32,33] Once the ordering of lamellae is complete, the domains enter the growth stage where domains increase in size by coalescence and dissolution.[14,32,34,35] The growth of the domains vs annealing time follows a power, $R \propto t^\alpha$, where R is the radius of the domain and t is annealing time.[32,34,35] The theoretical value of α has been shown to equal $^1/_3$ for ideal films,[35,36] but experimentally determined values of α are less than $^1/_4$.[32,34,35] Grim et al. showed that multilayered domain structures and line defects reduce theoretical values of α, and thus, slow the formation and growth of the relief structures.[35]

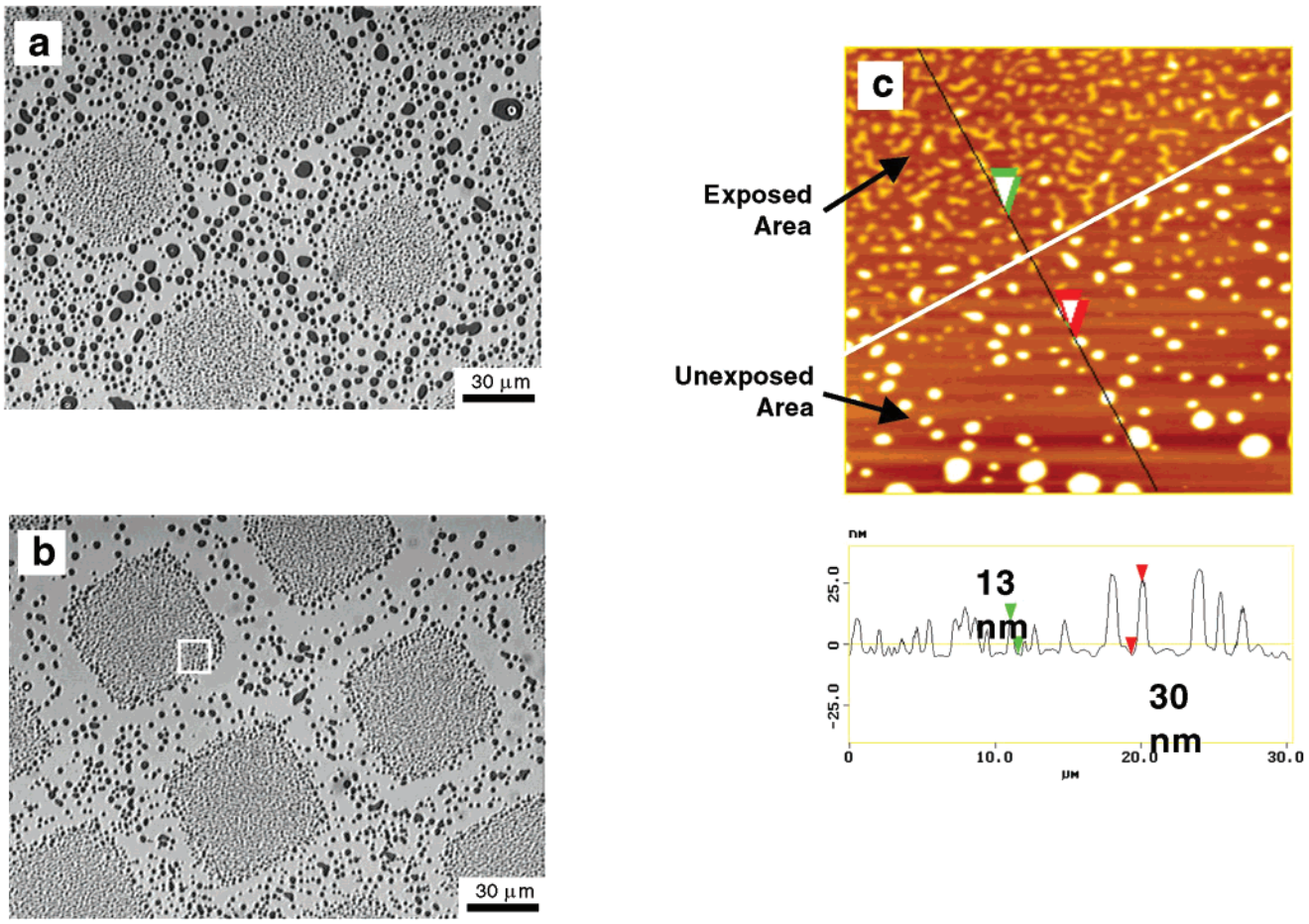

Figure 2. Optical micrographs of films of P(S-*b*-MMA) on patterned OTS exposed to X-rays at doses of (a) 800 mJ/cm^2 and (b) 900 mJ/cm^2. The initial thickness of both films was 2.2L_o. (c) Higher resolution AFM image of the outlined area in part b and a cross-sectional profile showing step heights of the islands. The area above the white line is the exposed area, and the area below the white line is the unexposed area. The step height of islands in the exposed area ($\sim$ 13 nm) was much less than the 30 nm (L_o) step height of islands in the unexposed area.

On the basis of these results, we believe the islands over exposed regions in the films shown in Figure 2 are still in the formation stage after annealing for 24 h, and the islands over unexposed regions are in the growth stage. The islands over exposed regions must have a lower rate of formation than the islands over unexposed regions, and this lower rate is most likely due to increased number of defects in the lamellar structure over exposed regions.

An increased defect-density in the lamellar structure of the polymer films over exposed regions is inferred to be due to a small difference in the interfacial energies between exposed OTS and the PS and PMMA blocks. The interactions between the blocks of the copolymer and the substrate determine the wetting behavior and the underlying lamellar structure in the film. On surfaces of OTS exposed to doses between 800 and 900 mJ/cm^2, $\Delta\gamma$ was small such that the energetic penalty for the presence of both blocks at the substrate was low, and the formation of defects is more likely than on surfaces where $\Delta\gamma$ is large. Defects may decrease the rates of the ordering process and the formation of topography in several ways: (1) by acting as sites for stress relaxation of polymer chains, (2) by accommodating excess material that would otherwise form islands on the surface of the film, and (3) by reducing the line tension of islands or holes. $\Delta\gamma$ is also the driving force for the formation of well-ordered parallel lamellae and the healing of defects. Thus, low values of $\Delta\gamma$ result in slower kinetics for the lamellar-ordering process and slower kinetics for the formation of islands or holes. Defects also will slow the kinetics of the growth process of surface domains due to the reduced line edge tension that is the driving force for coalescence. It is expected that, with increased annealing time of the films shown in Figure 2, the lamellar-ordering process would be completed over the exposed regions such that defects are annihilated and the islands enter the growth stage where their step height would equal L_o.

Symmetric Wetting/Neutral Wetting Patterns. Two optical micrographs of thin films of P(S-*b*-MMA) of different thicknesses deposited and annealed on patterned OTS exposed to X-rays at a dose of 1000 mJ/cm^2 are shown in Figure 3, parts a and b. This dose is approximately equal to the neutral dose for SA films of OTS. Islands formed over unexposed OTS on the film in Figure 3a, and a bicontinuous topography formed over unexposed OTS on the film in Figure 3b. Islands and bicontinuous topography were consistent with symmetric wetting of the P(S-*b*-MMA) film over unexposed OTS for initial film thicknesses of 2.2L_o and 2.5L_o, respectively. The exposed regions in both of these films remained flat and featureless, characteristic of neutral wetting with the lamellae oriented perpendicular to the plane of the film. Plane-view TEM confirmed the perpendicular orientation of the lamellae over the

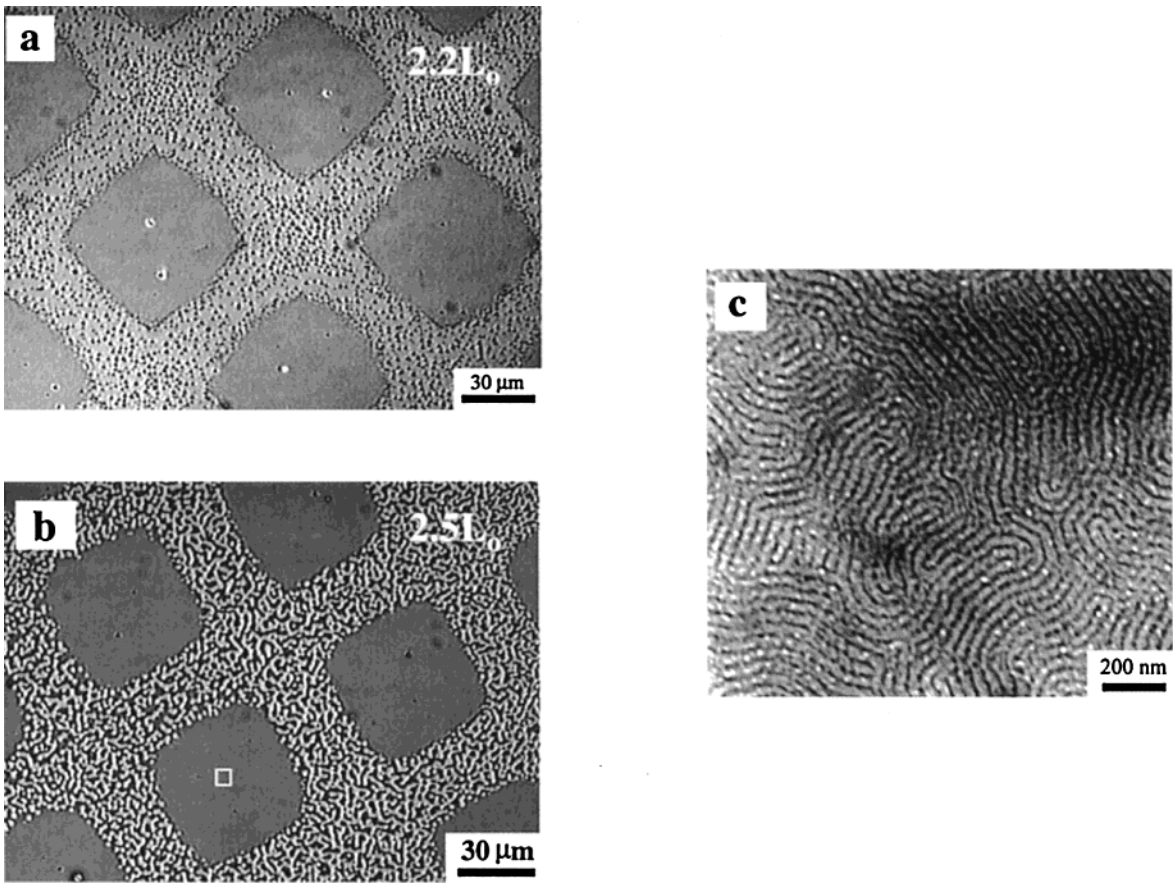

Figure 3. Optical micrographs of two films of P(S-*b*-MMA) on patterned OTS exposed to X-rays at a dose of 1000 mJ/cm^2. The initial thicknesses of the films were (a) $2.2L_o$ and (b) $2.5L_o$. (c) A plane-view TEM image of the outlined area in part b. The PS block appears darker due to staining with RuO_4. The alternating light and dark regions confirm an orientation of the lamellae perpendicular to the substrate.

exposed regions of the films (Figure 3c). The contrast in the image was due to staining of the PS domains with RuO_4. An AFM image of the film depicted in Figure 3a is shown in Figure 4a. From the cross-sectional profile, the height difference between exposed and unexposed areas was ~2 nm. This step height was less than $^1/_2L_o$, the step height between symmetric wetting/asymmetric wetting patterns as shown previously[23,28,31] and in the next section. An LFM image of the film, shown in Figure 4b, over an exposed region of the OTS showed lamellae with perpendicular orientation. The contrast in the LFM image is due to differences in elasticity, adhesive and frictional forces with the AFM tip, and other forces due to the different chemical composition between the PS and PMMA domains.

LFM images of three islands on the film shown in Figure 4a are shown in Figure 5. The island in Figure 5a was 5.5 μm from the symmetric wetting/neutral wetting boundary as defined in Figure 4; the island in Figure 5b was 8.0 μm from the pattern boundary; the island in Figure 5c was 12.3 μm from the pattern boundary. Perpendicular lamellae were detected at the edge of the islands in Figure 5, parts a and b, but not for the island in Figure 5c. For the island in Figure 5a, perpendicular lamellae were detected in a ring ~0.5 μm in width around the island. For the island in Figure 5b, the width of the ring of perpendicular lamellae was only ~0.1 μm. From the cross-sectional profiles of the three islands, the slope of the island edge increased with increasing distance from the symmetric wetting/neutral wetting boundary. The step height of the island in Figure 5a was slightly less than L_o (27 nm = $0.9L_o$).

Liu et al. have shown that the edge profile of islands depends greatly on the surface tension.[37] The surface tension applies a strong force to flatten the edge profile resulting in compression of lamellae or a transition in the orientation of lamellae from parallel to perpendicular at the island edge. When the value of $\Delta\gamma$ is small, it may be energetically more favorable for the lamellae to undergo a transition in orientation than to be compressed. Near the wetting/pattern boundary on the unexposed side of the film in Figure 4a, $\Delta\gamma$ was small, and the lamellae at the island edge were oriented perpendicular. The perpendicular orientation allowed flattening of the edge profile such that the step height did not reach the maximum value of 30 nm. With increasing distance from the wetting/pattern boundary, $\Delta\gamma$ increased, and compression of lamellae became energetically more favorable than a transition in the orientation.

Symmetric Wetting/Weakly Asymmetric Wetting Patterns: Size of Hole Topography Depending on Interfacial Energy. Two optical micrographs of thin films of P(S-*b*-MMA) deposited and annealed on patterned OTS exposed to X-rays at doses of 1100 and 1200 mJ/cm^2 are shown in Figure 6, parts a and b, respectively. These doses are slightly greater than the neutral dose for SA films of OTS. An AFM image and cross-sectional profile of a region of the film over an exposed area in Figure 6a is shown in Figure 6c. Islands formed over unexposed areas of the OTS, and holes formed over exposed areas of the OTS. For the initial thickness of $2.2L_o$, island formation was indicative of symmetric wetting and hole formation was indicative of asym-

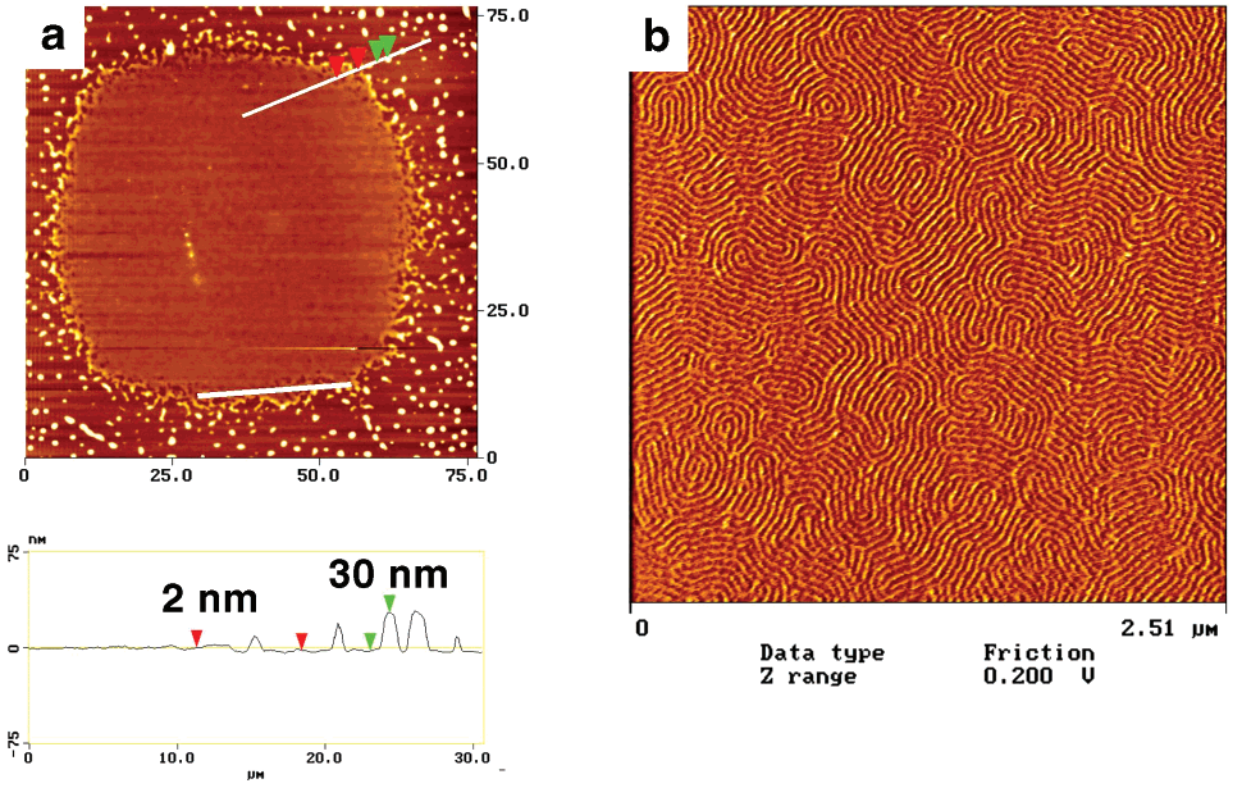

Figure 4. (a) AFM image and cross-sectional profile of the film from part a of Figure 3. The step height between exposed and unexposed regions was 2 nm. The pattern boundary between exposed and unexposed regions is defined by the white line. (b) LFM image of surface of the film over exposed regions. Perpendicular lamellae were detected at the surface of the film showing that the perpendicular orientation extended throughout the thickness of the film.

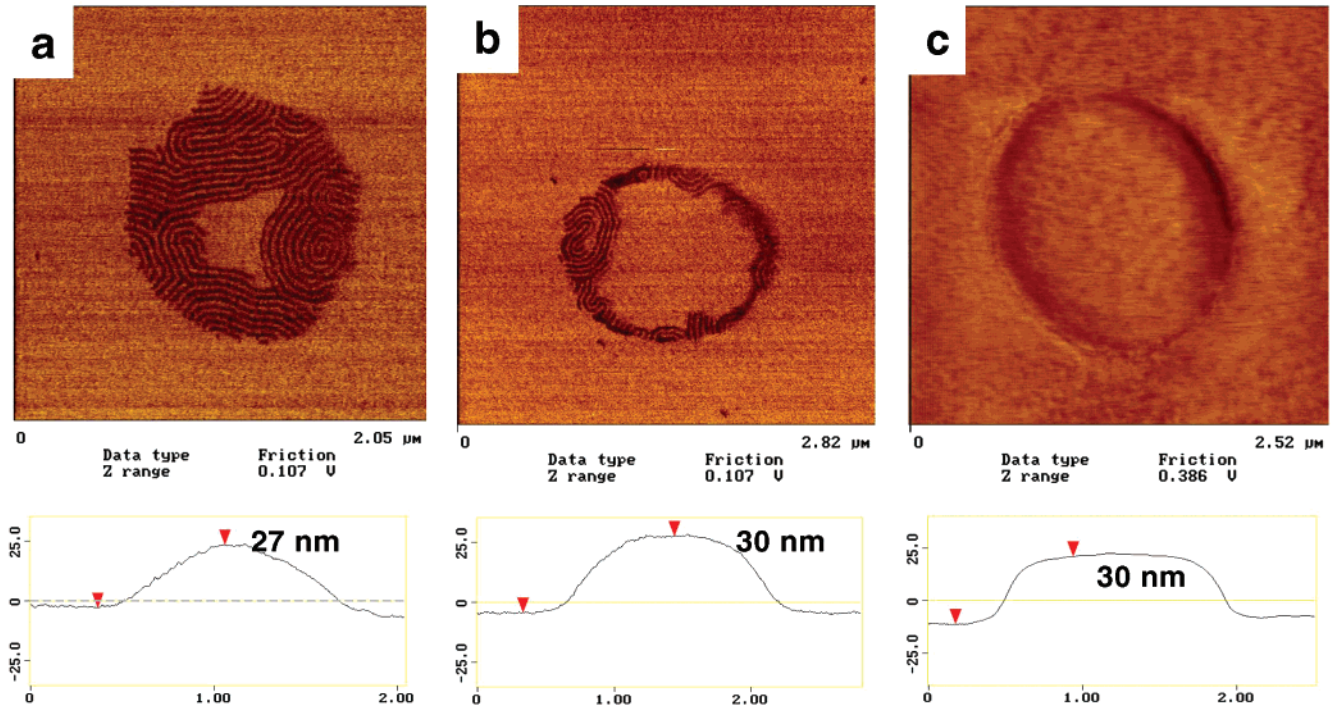

Figure 5. (a) LFM image of island located 5.5 μm from the pattern boundary on the unexposed side. An ~0.5-μm-wide ring of perpendicular lamellae was detected at the island edge. The step height of the island was 27 nm. (b) LFM image of island located 8.0 μm from the pattern boundary on the unexposed side. An ~0.1-μm-wide ring of perpendicular lamellae was detected at the island edge. The step height of the island was 30 nm. (c) LFM image of island located 12.3 μm from the pattern boundary on the unexposed side. No perpendicular lamellae were detected at the edge of the island. The step height of the island was 30 nm.

metric wetting. The average area of the holes for a dose of 1100 mJ/cm^2 (0.66 μm^2) was less than the average area of the holes for a dose of 1200 mJ/cm^2 (5.1 μm^2). From the AFM cross-sectional profile shown in Figure 6c, the step height of the holes in 6a was ~13 nm compared to a step height of 30 nm for the holes in

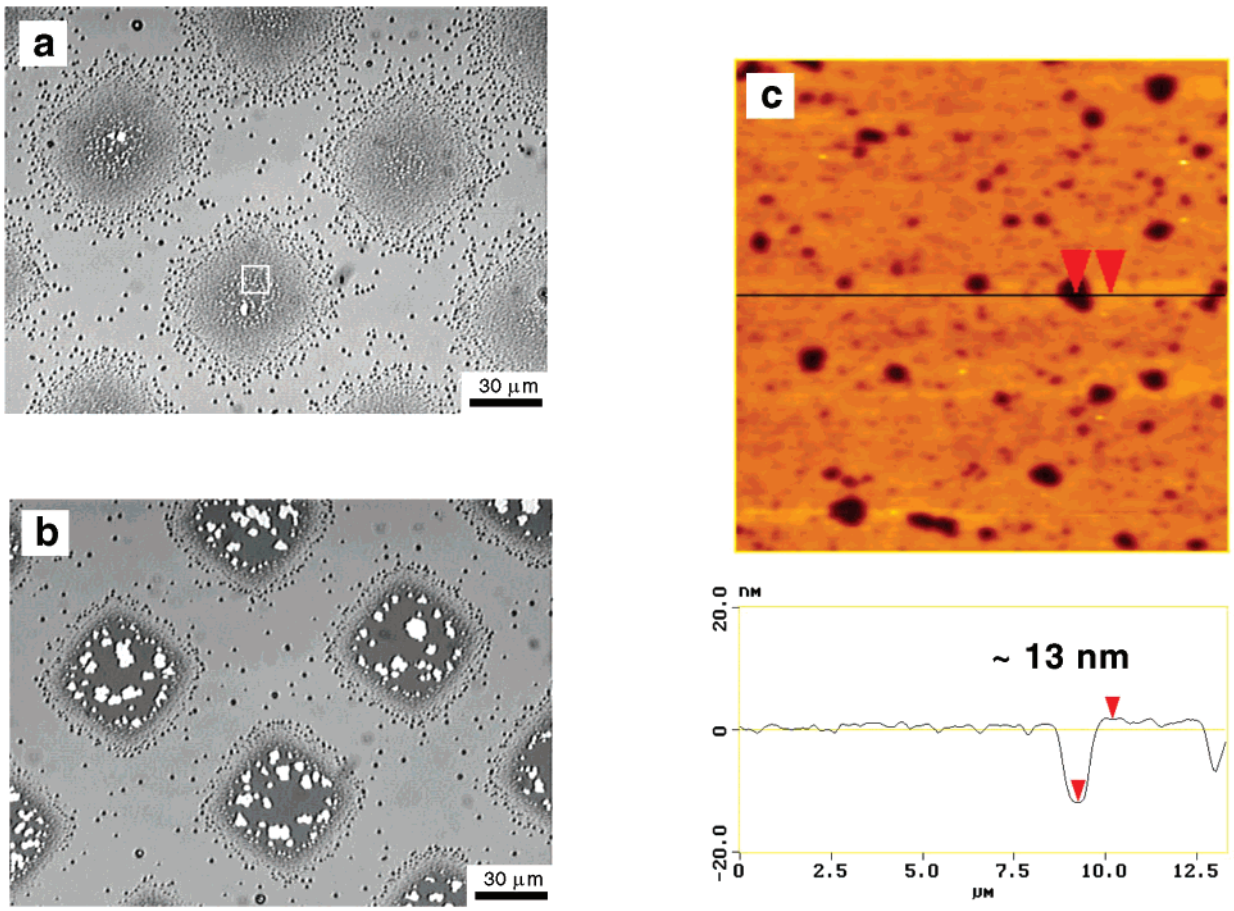

Figure 6. Optical micrographs of two films of P(S-*b*-MMA) on patterned OTS exposed to X-rays at doses of (a) 1100 and (b) 1200 mJ/cm^2. The initial thickness of both films was $2.2L_o$. (c) Higher resolution AFM image of the outlined area in (a) and a cross-sectional profile showing the step height of the holes equals ~13 nm.

Figure 6b (AFM data not shown). The value of 13 nm for the step height of holes in Figure 6a is approximately $^1/_2L_o$, but to our understanding this value has no physical significance and is arbitrarily less than L_o depending upon the annealing time for the film.

Similarly, as for the islands over exposed regions shown in Figure 2, we believe the holes over exposed regions of the film depicted in Figure 6a are still in the formation stage, and the holes over exposed regions of the film depicted in Figure 6b are in the growth stage. At a dose of 1100 mJ/cm^2, $\Delta\gamma$ is small, and the formation of defects is more likely than at a dose of 1200 mJ/cm^2. These defects reduce the rate of formation and growth of the surface relief structures; thus, the holes in the formation stage will have step heights less than L_o and will have smaller areas. It is expected that with increased annealing time beyond 24 h, the lamellar-ordering process over exposed regions of the film shown in Figure 6a would be completed such that the lamellar structure becomes well-ordered and the holes enter the growth stage where their step height would equal L_o.

Symmetric Wetting/Asymmetric Wetting Patterns: Effect of Varying Initial Film Thickness. We investigated the wetting behavior of films of P(S-*b*-MMA) on patterned OTS exposed to X-rays at doses greater than 1400 mJ/cm^2. These doses were much greater than the neutral dose for SA films of OTS. On these samples the lamellae were likely well-ordered and parallel over both exposed and unexposed regions due to large magnitudes of $\Delta\gamma$ for both exposed and unexposed regions. Large scale optical micrographs of annealed thin films of P(S-*b*-MMA) with thicknesses from approximately $1.75L_o$ (53 nm) to approximately $2.75L_o$ (82 nm) on OTS patterned with doses ranging from 1400 to 2000 mJ/cm^2 are shown in Figure 7. Figure 8 shows AFM images of single squares from the films. These films are representative of many samples with the same thicknesses and morphologies. Island or hole formation was determined from the AFM images. The morphologies of the films are described in Table 1. Cross-sectional profiles from four of the AFM images in Figure 8 are shown in Figure 9. In all cases, the thickness difference between the exposed and unexposed regions was ~15 nm ($^1/_2L_o$), and the step height of islands and holes was ~30 nm (L_o).

The wetting behavior of the films in Figure 4 was analyzed by using the formation of topography, the type of topography, i.e., island, holes, or bicontinuous, and the initial film thickness. In Figure 7, parts a−e, g, and i, the observed topography on the film surface over the exposed regions was consistent with asymmetric wetting for each initial thickness. The observed topography on the film surface over the unexposed regions in Figure 7, parts a, c, and e−i was consistent with symmetric wetting for each initial thickness. The thickness difference of $^1/_2L_o$ between exposed and unexposed regions was equal to the difference in quantized thickness between symmetric (nL_o) and asymmetric ($(n + {}^1/_2)L_o$) wetting.

Evolution of Pattern Morphology in P(S-*b*-MMA) films. The evolution of pattern formation was studied as a function of annealing time. Figure 10 shows an

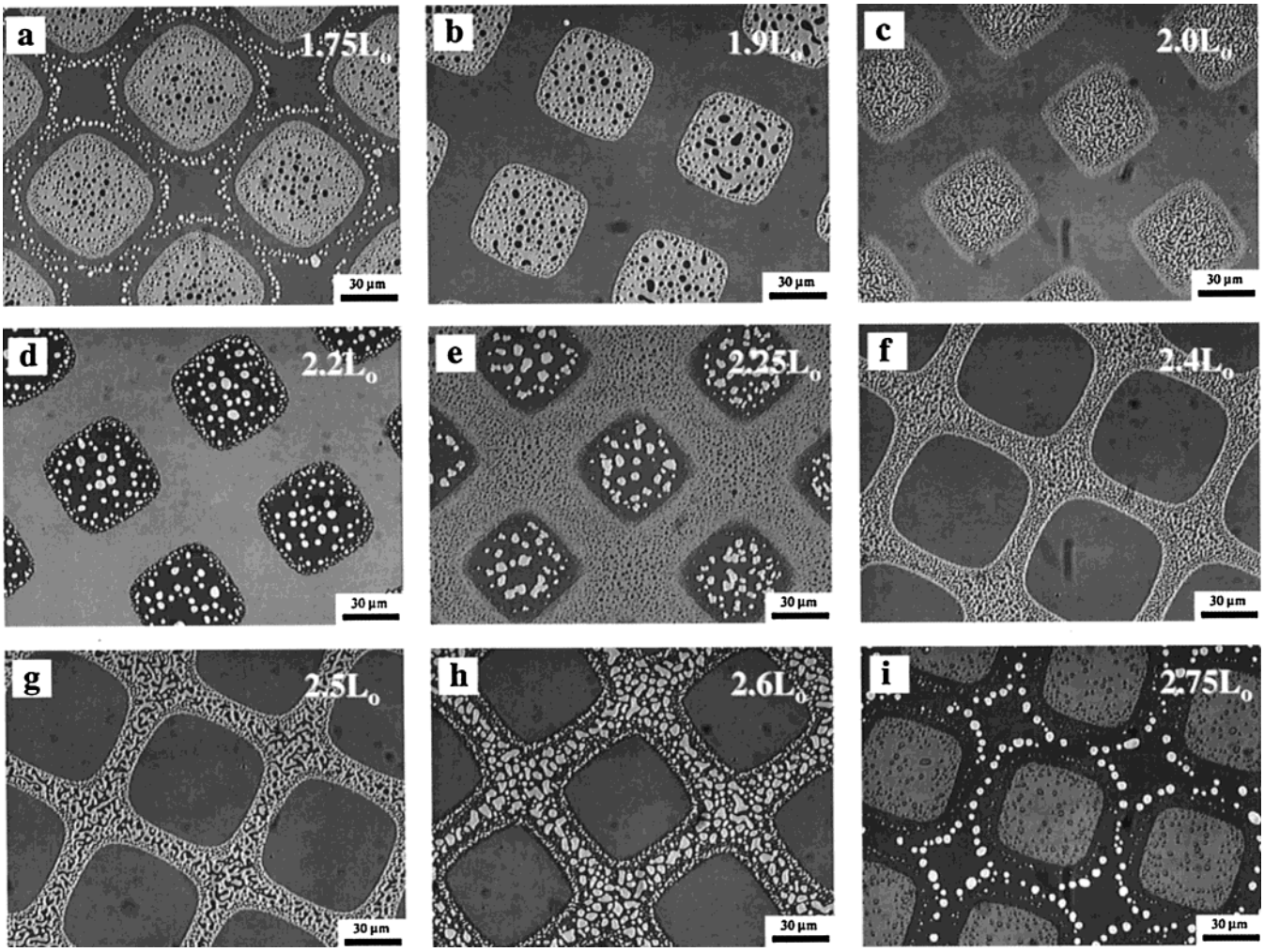

Figure 7. Optical micrographs of thin films of P(S-*b*-MMA) deposited on patterned OTS exposed to X-rays through a 300 mesh nickel grid at doses from 1400 to 2000 mJ/cm^2. Initial film thicknesses: (a) 53 nm = 1.75L_o; (b) 57 nm = 1.9L_o; (c) 60 nm = 2.0L_o; (d) 66 nm = 2.2L_o; (e) 68 nm = 2.25L_o; (f) 72 nm = 2.4L_o; (g) 75 nm = 2.5L_o; (h) 78 nm =2.6L_o; (i) 82 nm = 2.75L_o.

optical micrograph of a thin film deposited on patterned OTS immediately after spin coating. Thickness variations estimated to be on the order of 1−3 nm (∼0.1L_o) existed across the film, and these variations mirrored the chemical pattern of the surface. These thickness variations were not detectable by AFM due to the diffuse boundary and shallow gradient in thickness. Figure 11 shows a series of AFM images of the film of P(S-*b*-PMMA) from Figure 7h. The film was annealed on a hot stage for different time steps with AFM performed after each step. After only 5 min of annealing at 180 °C, the chemical surface pattern was observable in the polymer film. The pattern boundaries and pattern dimensions were the same after 5 min of annealing as after 23 h of annealing (Figure 11e). This fact and Figure 10 suggest that the pattern boundaries were set during the spin coating process or within the first moments of annealing. Over exposed regions (asymmetric wetting) in Figure 11a, the film was flat and featureless. Surface roughness did not appear, develop into islands, and disappear after longer annealing as observed in the experiments of Heier et al.[26,27] This result seems to indicate coordination of the different regions of the film during the early stages of ordering that result in a morphology that mirrors the morphology of the film during late stages of annealing. We do not understand the mechanism of this coordination process. Over unexposed regions (symmetric wetting), two regimes were visible. In the center of the film over unexposed regions, hole formation had started with the holes having step heights of ∼26 nm (0.87L_o). Over unexposed regions next to the pattern boundary, surface roughness with a height of ∼3 nm was present. After 15 min of annealing, the pattern in the polymer film was further developed. Again, the film over exposed regions was flat and remained flat for the remainder of annealing times. Over unexposed regions of OTS, the two regimes were still present. Near the center of the unexposed regions, holes were well-developed with a step height of 30 nm (L_o) and were beginning to coalesce. During further annealing, the holes in these regions only grew larger. However, a 4-μm-wide transition region still existed on the unexposed side of the pattern boundary. This transition region with surface roughness of ∼3 nm was present up to 105 min of annealing. After 23 h of annealing, the roughness in the transition region developed into holes with step heights of 30 nm.

The holes in the unexposed and transition regions of the film in Figure 11 have different rates of formation and growth. The holes over unexposed regions entered the growth stage after 15 min of annealing at 180 °C. For longer annealing times, these holes grow by coalescence and dissolution. Holes in the 4-μm-wide transition region remained in the formation stage for at least 105 min of annealing. After 23 h, the holes in the transition region had entered the growth stage. The

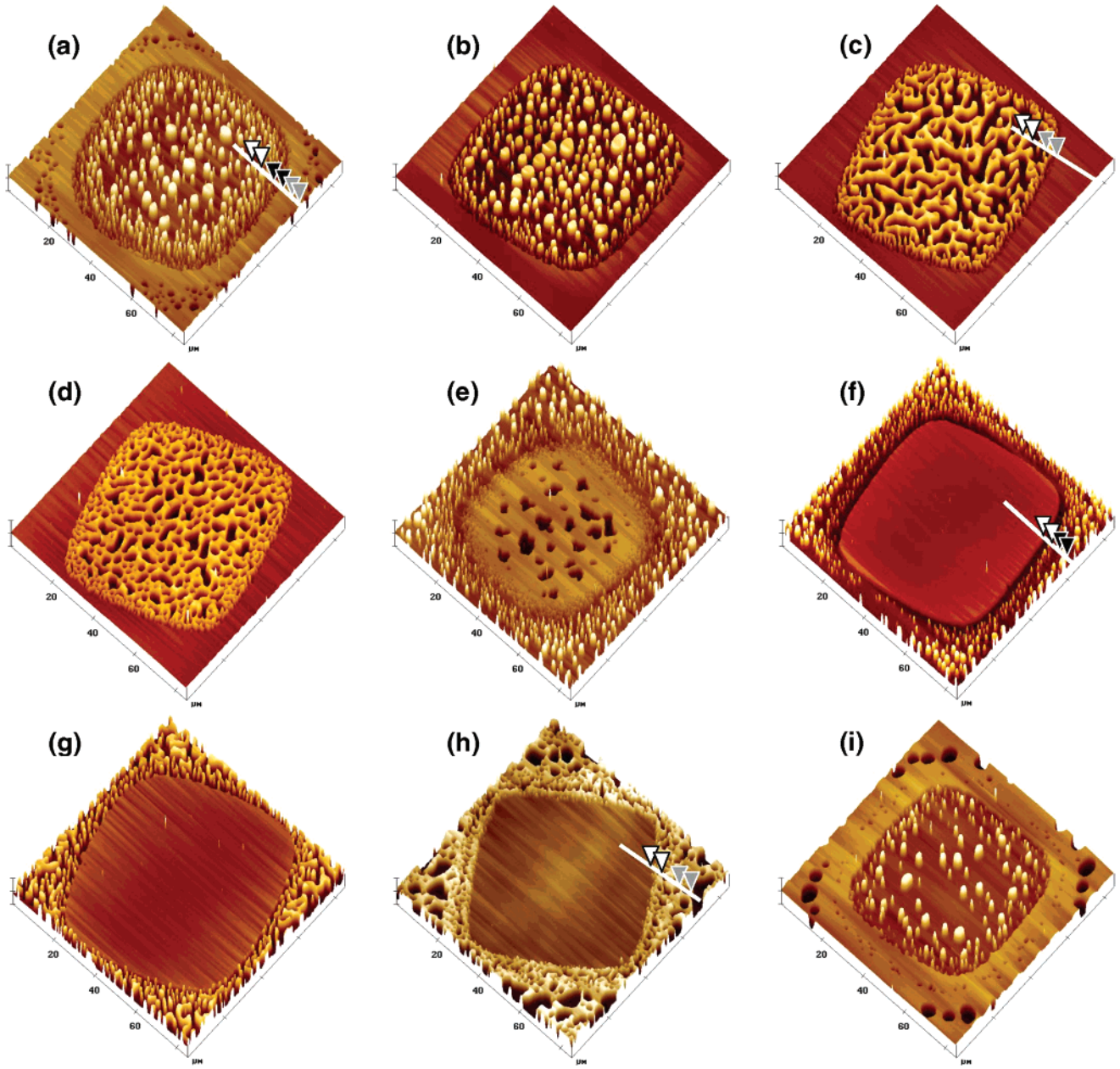

Figure 8. AFM images of thin films of P(S-*b*-MMA) from Figure 7. Initial film thicknesses: (a) 53 nm = 1.75L_o; (b) 57 nm = 1.9L_o; (c) 60 nm = 2.0L_o; (d) 66 nm = 2.2L_o; (e) 68 nm = 2.25L_o; (f) 72 nm = 2.4L_o; (g) 75 nm = 2.5L_o; (h) 78 nm =2.6L_o; (i) 82 nm = 2.75L_o. The lines in parts a, c, h, and i show the scan lines for the cross-sectional profiles in Figure 9. The height scale is 50 nm for all of the images.

Table 1. Initial Film Thicknesses and Morphologies over Unexposed and Exposed Regions of the P(S-*b*-MMA) Films Shown in Figure 7

figure	initial thickness	morphology over unexposed regions	morphology over exposed regions
7a	53 nm = 1.75L_o	holes	islands
7b	57 nm = 1.9L_o	flat	islands
7c	60 nm = 2.0L_o	flat	bicontinuous
7d	66 nm = 2.2L_o	flat	holes
7e	68 nm = 2.25L_o	islands	holes
7f	72 nm = 2.4L_o	islands	flat
7g	75 nm = 2.5L_o	bicontinuous	flat
7h	78 nm = 2.6L_o	holes	flat
7i	82 nm = 2.75L_o	holes	islands

slower rates of formation and growth of the holes in the transition region may be due to a high defect-density in the lamellar structure of the film in this region. These defects are more likely in the transition region because of smaller values of $\Delta\gamma$. Rates of formation and growth also depend on the difference in the initial film thickness and the quantized value of thickness.[32,33,35] As this difference increases, the rates of formation and growth of surface relief structures increase. A thickness gradient from exposed to unexposed regions due to thickness differences that are present immediately after spin coating (see Figure 10) might be responsible for the different rates of formation and growth of the holes on the film shown in Figure 11. A transition region with smaller average domain size is present in most of the films shown in Figure 7, possibly indicative of slower rates of formation and growth in these regions.

Regions of Films Remaining Flat When Thickness Does Not Equal Quantized Value. In Figure 7, parts b, d, f, and h, regions of the films (either over exposed or unexposed areas of the OTS) remained flat

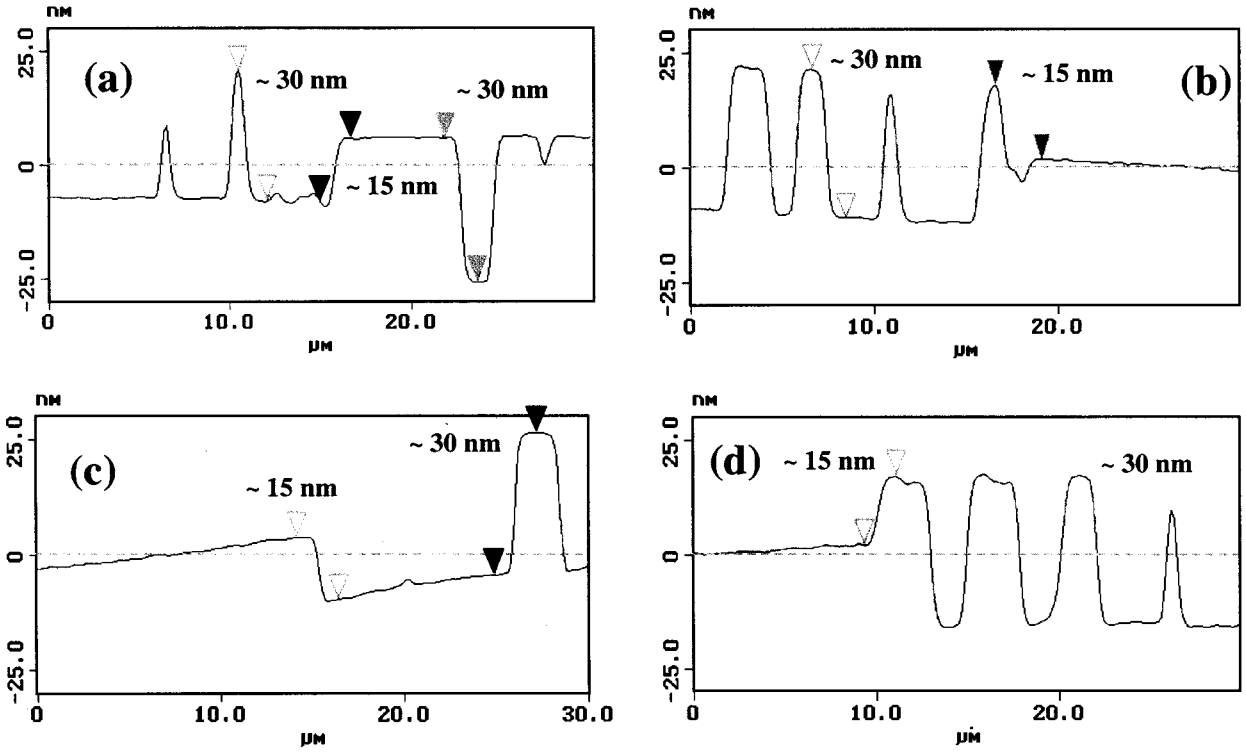

Figure 9. Selected cross-sectional profiles from AFM images from Figure 8. For each film, the step height of domains (either islands or holes) was ~30 nm = L_o, and the step height between square areas and bar areas was ~15 nm = $^1/_2L_o$. Key: (a) part a of Figure 8; (b) part c of Figure 8; (c) part f of Figure 8; and (d) part h of Figure 8.

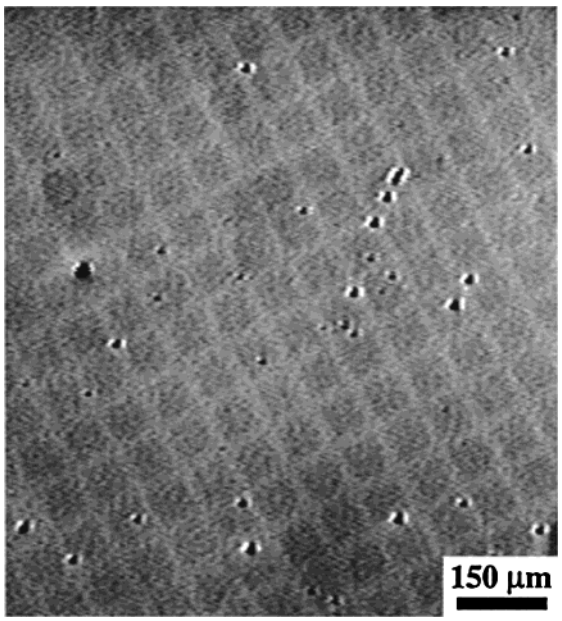

Figure 10. Optical micrograph of unannealed thin film of P(S-*b*-MMA) on micropatterned OTS. The contrast is due to thickness differences in the film of ~1−3 nm.

even though $t \neq t_n$ for either symmetric or asymmetric wetting for any of the films. The flat areas are not due to perpendicular orientation of lamellae in these regions of the films. Lamellae do not orient perpendicular over unexposed OTS or over OTS exposed to doses greater than 1200 mJ/cm^2, and the lack of perpendicular lamellae was verified using TEM (data not shown). Four possibilities to explain the presence of these flat regions are as follows: (1) the initial film thickness actually equaled t_n, (2) thickness variations across the film occurred during spin coating, (3) compression or expansion of lamellae took place, and (4) mass transport of material between symmetric and asymmetric wetting regions was observed.

On the patterned surfaces, the quantization of film thickness results in a $^1/_2L_o$ difference in thickness between adjacent symmetric and asymmetric wetting regions. If the thickness equals t_n for one type of wetting region such that this region of the film is flat, the thickness in the adjacent region is $t_n + {}^1/_2L_o$ such that bicontinuous morphology forms. Smith et al. studied the morphology as a function of film thickness of the same block copolymer used in this paper (P(S-*b*-MMA) with $M_n = 51$ kg/mol purchased from Polymer Source, Inc.).[38] They deposited thin films of the copolymer on silicon wafers using an automated solution flow coater that uses a knife edge and a computer-controlled, variable-speed stage to spread the solution at constant acceleration producing a continuous film with a nonlinear gradient in thickness. Several films with different thicknesses and gradients were deposited on the same wafer and annealed, thus allowing Smith et al. to study the effects of thickness on the morphology of the P(S-*b*-MMA) films on one substrate. They found a large thickness range over which bicontinuous or serpentine topography was observed. For asymmetric wetting conditions, this thickness range was 54−61 nm (1.8−2.0L_o). For the films shown in Figure 7, parts b, d, f, and h, the nonflat regions did not exhibit bicontinuous morphology; these regions exhibited circular islands and holes characteristic of film thicknesses far from t_n. Therefore, these films most likely had thicknesses at least 0.2L_o greater than or less than t_n. It is, therefore, unlikely that the thicknesses of the flat regions in these films equaled t_n.

Thickness variations in the film that occurred during spin coating (see Figure 10) cannot consistently explain the presence of flat regions when $t \neq t_n$, assuming one region of the film (either over exposed or unexposed)

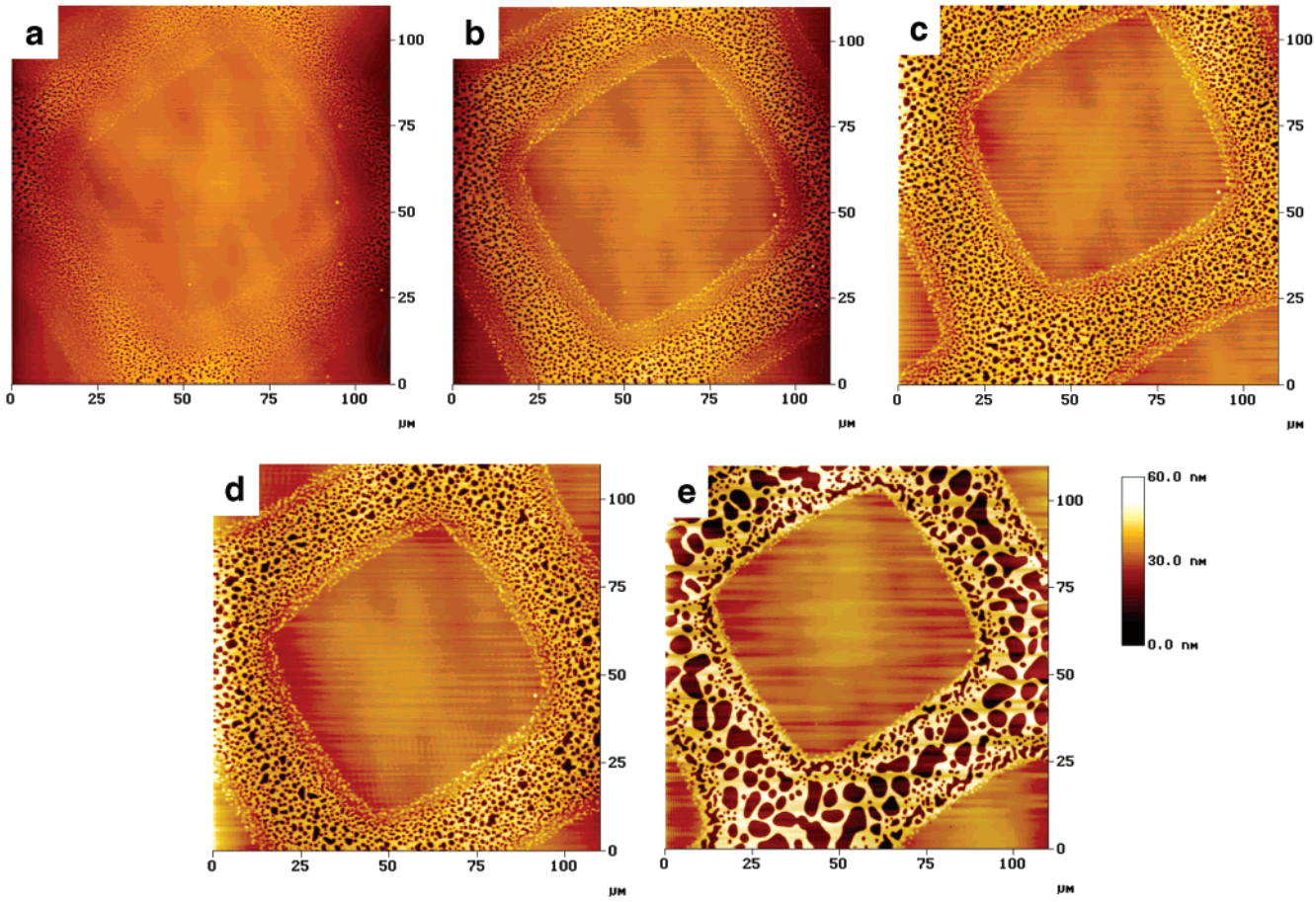

Figure 11. AFM images of the film from Figure 7h at different times during the annealing process: (a) 5 min of annealing; (b) 15 min of annealing; (c) 45 min of annealing; (d) 105 min of annealing; and (e) 23 h of annealing.

was always 3 nm thicker or thinner than the adjacent region of the film after spin coating. We could not determine conclusively whether exposed or unexposed regions of the film were always thicker or thinner than the other regions, and we will consider each case below. For example, consider two films of nominal thicknesses $1.9L_o$ and $2.4L_o$, and assume the thickness of the film over the exposed regions is 3 nm thicker ($2.0L_o$ and $2.5L_o$, respectively) than the film over the unexposed regions. For the nominal $2.4L_o$ film, the topography would be flat over exposed regions ($2.5L_o$) and islands over unexposed regions ($2.4L_o$). This description is the morphology of the film shown in Figure 7f. For the nominal $1.9L_o$ film, the film topography would be bicontinuous over exposed regions ($2.0L_o$) and holes over unexposed regions ($1.9L_o$). This description, however, is not the morphology of the film shown in Figure 7b (holes over exposed regions and flat over unexposed regions). Next, consider again two nominal film thicknesses of $1.9L_o$ and $2.4L_o$, and assume the thickness of the film over the unexposed regions is 3 nm thicker ($2.0L_o$ and $2.5L_o$, respectively) than the film over the exposed regions. For the nominal $1.9L_o$ film, the film topography would be flat over unexposed regions ($2.0L_o$) and islands over exposed regions ($1.9L_o$). This description is the morphology of the film shown in Figure 7b. For the nominal $2.4L_o$ film, the topography would be bicontinuous over unexposed regions ($2.5L_o$) and holes over exposed regions ($2.4L_o$). This description is not the morphology of the film shown in Figure 7f (islands over unexposed regions and flat over exposed regions). One can also consider the cases where the film over exposed regions is always thinner than the film over unexposed regions or the film over unexposed regions is always thinner than the film over exposed regions. Both of these two scenarios give accurate descriptions of film morphologies for some initial thicknesses but not for all initial thicknesses. The thickness variations that occur during spin coating are more likely responsible for the alignment of topography next to the pattern boundary as in Figure 7, parts a and i, and are not responsible for the presence of the flat regions.

Lamellae may be compressed or stretched from their equilibrium conformation in the flat regions. Smith et al. observed flat regions in asymmetric-wetting-films of symmetric P(S-*b*-MMA) when the film thickness was $(n + {}^1/_2)L_o \pm 0.15L_o$. for thicknesses ranging from 1.5 to $6.5L_o$.[38] They concluded the large range over which the films remained flat was due to deformations in chain conformations in the outer layer of copolymer molecules that resulted in swelling or shrinking of the film thickness. They based this conclusion on (1) insensitivity of $\Delta h/L_o$ to M, where Δh is the change in film thickness across the entire flat region,and (2) changes in the interference colors of a P(S-*b*-MMA) film with $M_n = 104$ kg/mol as the thickness increased 25 nm from 2.2 to $2.8L_o$. We observed flat and featureless films for symmetric-wetting regions for initial film thicknesses of $1.9-2.2L_o$ and for asymmetric-wetting regions for initial film thicknesses of $2.4-2.6L_o$. The thickness ranges over which flat regions were observed in the work of Smith et al. and in our work are comparable.

Several extenuating facts, however, suggest that the results of Smith et al. are sensitive to the molecular

mass of the copolymer. (1) Lamellar deformations become increasing likely compared to island or hole formation with increasing M. Russell et al. observed swelling of the outer layer of a $1.7L_o$-thick film of P(S-*b*-MMA) with $M_n = 300$ kg/mol, and they concluded the swelling occurred instead of island formation because of the high value of M.[39] (2) Islands and holes form more slowly with increasing M.[40] (3) For the P(S-*b*-MMA) with $M_n = 104$ kg/mol used by Smith et al., the mobility may be small such that the polymer film is effectively pinned to the substrate and acts like a surface-grafted polymer brush as discussed by Smith et al. (4) There was no observed color change for a P(S-*b*-MMA) film with $M_n = 26$ kg/mol for thickness changes of approximately 5 nm from 3.4 to $3.7L_o$, from 4.4 to $4.7L_o$, or from 5.4 to $5.7L_o$. A 5-nm change in thickness, perhaps, may not be able to be perceived by the human eye. The P(S-*b*-MMA) with $M_n = 26$ kg/mol is less likely to have lamellar deformations than the P(S-*b*-MMA) with $M_n = 104$ kg/mol. The high mobility and ease of island formation for the low-M polymer suggest that another explanation besides lamellar deformation may be responsible for the flat regions for the P(S-*b*-MMA) with $M_n = 26$ kg/mol.

Heier et al. studied the behavior of $1.7L_o$-thick films of poly(styrene-*b*-2-vinylpyridine) with $M_n = 200$ kg/mol on chemically patterned surfaces.[24−27] In these studies, they observed the formation of islands that disappeared with increased annealing time for asymmetric-wetting regions of the films. They concluded the disappearance of the islands was due to mass transport of the copolymer molecules from regions of excess (island-forming regions) to absorbing boundary regions with high defect-density in the lamellar structure. Mass transport of excess material also is likely to explain the presence of the flat regions in the films shown in Figure 7, parts b, d, f, and h. There is a strong driving force in the thin films to achieve the bulk lamellar period and t_n as dictated by symmetric and asymmetric wetting. On a homogeneous surface, the film can only form islands or holes locally to meet the quantized thickness and maintain a constant lamellar period. On the patterned surfaces, symmetric wetting and asymmetric wetting regions exist next to each other, and these regions can exchange material to allow one region to reach its desired thickness resulting in a global minimization of the total free energy. The copolymer molecules in a region that has a slight excess of material, e.g., $2.2L_o$ thickness over symmetric wetting region, and that would form islands on a homogeneous substrate has an available sink that will accept this excess material and allow this region to meet its quantized thickness, i.e., $2.0L_o$. The sink, an asymmetric wetting region over an exposed area in this case, accepts this excess material because it is trying to complete its upper layer with a thickness of $2.5L_o$. However, the excess material that it accepts is not enough to complete its upper layer, and holes still form. The opposite also can occur. Regions with slight deficits of material, e.g., $2.4L_o$ thickness over asymmetric wetting region, can take material away from an adjacent island-forming region. Material moves from regions with excesses toward regions with deficits, and whichever region is closer to its preferred thickness will be flat and featureless. This direction of transport is in agreement to that reported by Heier et al.[25−27] The presence of the transition region between symmetric and asymmetric wetting regions and the defects within may affect transport of excess material in several ways. (1) The defects may act as channels to allow excess material to be exchanged across the pattern boundary. These defect-channels would be similar to channels proposed by Mayes et al. to describe the flow of copolymer molecules in films on homogeneous surfaces during the ordering of lamellae parallel to surfaces.[16] In our case, the channels would be oriented parallel to the plane of the film to allow transport of material between neighboring wetting regions. (2) The defect-rich region may act as an absorbing region for excess material. This type of behavior would be similar to the behavior observed by Heier et al.[26,27] (3) The defect-rich region may act as a temporary depot to store excess material before it is absorbed by regions with deficits. For a polymer with high enough mobility (low enough M), mass transport is the more likely mechanism by which regions will remain flat. In the work of Smith et al.,[38] the thickness gradients in the films introduce sources and sinks for excess material to drive mass transport, and the flat regions of the films of P(S-*b*-MMA) with $M_n = 26$ kg/mol may be due to mass transport of excess material.

One remaining question is the mechanism for mass transport. To determine if molecular diffusion can explain the transport in the polymer films, we used values from the literature to estimate the self-diffusion coefficient of P(S-*b*-MMA). Several groups have shown that self-diffusion coefficients of diblock copolymers are an average of the self-diffusion coefficient of each of the constituent homopolymers of equivalent molecular mass to the block copolymer.[41,42] From Green et al., the self-diffusion coefficients of homopolystyrene ($M_n = 50\,000$ g/mol) and homo-poly(methyl methacrylate) ($M_n = 50\,000$ g/mol) were determined to be 6.8×10^{-11} and 9×10^{-14} cm^2/s at 180 °C, respectively.[43] From these data, we estimated the self-diffusion coefficient of P(S-*b*-MMA) to be 2.5×10^{-12} cm^2/s. Using dimensional analysis, we estimate that the length scale of molecular diffusion of P(S-*b*-MMA) is of order 0.2 μm after annealing at 180 °C for 2 h and 0.5 μm after annealing for 24 h. If we assume that the self-diffusion coefficient of P(S-*b*-MMA) equals the largest self-diffusion coefficient of the homopolymers, i.e., the self-diffusion coefficient of PS, then we estimate that the length scale of molecular diffusion for P(S-*b*-MMA) is on the order of 0.7 μm after annealing at 180 °C for 2 h and 2.4 μm after annealing for 24 h. These length scales are much smaller than the pattern features in our patterned copolymer films ($\sim$30 μm), and this result seems to discount molecular diffusion as the sole transport mechanism. Mass transport of excess material would have to rely on another mechanism such as pressure driven hydrodynamic flow.[26,27] Finally, it is possible that both lamellar deformations and mass transport may occur simultaneously. The molecular mass of the polymer probably plays an important role in determining which mechanism dominates, and this role is related to the mobility of the polymer and the ability of the polymer to form islands and holes. In the work of Smith et al.,[38] it is possible that mass transport governs the behavior of the P(S-*b*-MMA) with $M_n = 26$ kg/mol and lamellar deformations govern the behavior of P(S-*b*-MMA) with $M_n = 104$ kg/mol. The P(S-*b*-MMA) with $M_n = 51$ kg/mol used in this paper may undergo lamellar deformations and have mass transport of excess material.

Formation and Growth of Island/Hole Topography. The results presented in this paper primarily relate the formation and growth of islands and holes to interfacial energy between the substrate and the block copolymer film. We have shown that island and holes have slower rates of formation and growth when $\Delta\gamma$ is small than when $\Delta\gamma$ is large. Two other factors in addition to interfacial energy are largely responsible for the formation and growth of islands and holes: (1) film thickness[32,33,35] and (2) molecular mass.[38,40] All three parameters must be taken into consideration when studying thin films of block copolymers.

Conclusions

Self-assembled films of OTS on SiO_x/Si were chemically micropatterned with dimensions of 30 μm. Thin films of P(S-*b*-MMA) on the chemically micropatterned films of OTS replicated the surface pattern as topography due to differences in wetting behavior on the adjacent regions of the patterned surface. The interfacial energies between the blocks of the copolymer and the exposed regions of the OTS were varied by changing the exposure dose and altering the surface energy of the SA film. Over regions of the patterned surfaces where the value of $\Delta\gamma$ was small, P(S-*b*-MMA) films exhibited topography with smaller average areas and step heights after annealing for 24 h than topography that formed over regions of the patterned surface where the value of $\Delta\gamma$ was large. The smaller areas and heights were due to slower rates of formation and growth for the relief structures due to the presence of defects in the lamellar structure. On patterned surfaces where $\Delta\gamma$ was large for both unexposed and exposed regions, unexposed regions were preferentially wet by the PS block, and exposed regions were preferentially wet by the PMMA block. On these surfaces, the alternating wetting regions of the polymer film differed in thickness by a maximum of 15 nm ($^1/_2L_o$), which is equal to the difference in quantized thickness for symmetric and asymmetric wetting. The presence of flat regions of the film over either exposed or unexposed regions when $t \neq t_n$ may be due to either mass transport of excess material to regions with deficits of material or deformation of the lamellae in the outer layer of the polymer film.

Acknowledgment. Funding for this work was provided by the Semiconductor Research Corporation (Grant Number 98-LP-452), and a NSF Career Award (Grant Number CTS-9703207). Facilities were supported by DARPA/ONR (Grant Number N00014-97-1-0460) and the NSF (Grant Number DMR-0084402).

References and Notes

(1) Bates, F. S.; Fredrickson, G. H. *Annu. Rev. Chem.* **1990**, *41*, 525.
(2) Bates, F. S. *Science* **1991**, *251*, 898.
(3) Thurn-Albrecht, T.; Schotter, J.; Kastle, G. A.; Emley, N.; Shibauchi, T.; Krusin-Elbaum, L.; Guarini, K.; Black, C. T.; Tuominen, M.; Russell, T. P. *Science* **2000**, *290*, 2126.
(4) Thurn-Albrecht, T.; Steiner, R.; DeRouchey, J.; Stafford, C. M.; Huang, E.; Bal, M.; Tuominen, M.; Hawker, C. J.; Russell, T. P. *Adv. Mater.* **2000**, *12*, 757.
(5) Forster, S. *Ber. Bunsen-Ges.-Phys. Chem. Chem. Phys.* **1997**, *101*, 1671.
(6) Fogg, D. E.; Radzilowski, L. H.; Blanski, R.; Schrock, R. R.; Thomas, E. L. *Macromolecules* **1997**, *30*, 417.
(7) Leclere, P.; Parente, V.; Bredas, J. L.; Francois, B.; Lazzaroni, R. *Chem. Mater.* **1998**, *10*, 4010.
(8) Li, R. R.; Dapkus, P. D.; Thompson, M. E.; Jeong, W. G.; Harrison, C.; Chaikin, P. M.; Register, R. A.; Adamson, D. H. *Appl. Phys. Lett.* **2000**, *76*, 1689.
(9) Urbas, A.; Fink, Y.; Thomas, E. L. *Macromolecules* **1999**, *32*, 4748.
(10) Urbas, A.; Sharp, R.; Fink, Y.; Thomas, E. L.; Xenidou, M.; Fetters, L. J. *Adv. Mater.* **2000**, *12*, 812.
(11) Fink, Y.; Urbas, A. M.; Bawendi, M. G.; Joannopoulos, J. D.; Thomas, E. L. *J. Lightwave Technol.* **1999**, *17*, 1963.
(12) Anastasiadis, S. H.; Russell, T. P.; Satija, S. K.; Majkrzak, C. F. *Phys. Rev. Lett.* **1989**, *62*, 1852.
(13) Coulon, G.; Russell, T. P.; Deline, V. R.; Green, P. F. *Macromolecules* **1989**, *22*, 2581.
(14) Coulon, G.; Collin, B.; Ausserre, D.; Chatenay, D.; Russell, T. P. *J. Phys. Fr.* **1990**, *51*, 2801.
(15) Russell, T. P.; Coulon, G.; Deline, V. R.; Miller, D. C. *Macromolecules* **1989**, *22*, 4600.
(16) Mayes, A. M.; Russell, T. P.; Bassereau, P.; Baker, S. M.; Smith, G. S. *Macromolecules* **1994**, *27*, 749.
(17) Peters, R. D.; Yang, X. M.; Kim, T. K.; Sohn, B. H.; Nealey, P. F. *Langmuir* **2000**, *16*, 4625.
(18) Mansky, P.; Liu, Y.; Huang, E.; Russell, T. P.; Hawker, C. *Science* **1997**, *275*, 1458.
(19) Mansky, P.; Russell, T. P.; Hawker, C. J.; Mays, J.; Cook, D. C.; Satija, S. K. *Phys. Rev. Lett.* **1997**, *79*, 237.
(20) Mansky, P.; Russell, T. P.; Hawker, C. J.; Pitsikalis, M.; Mays, J. *Macromolecules* **1997**, *30*, 6810.
(21) Kim, T. K.; Yang, X. M.; Peters, R. D.; Sohn, B. H.; Nealey, P. F. *J. Phys. Chem. B* **2000**, *104*, 7403.
(22) Peters, R. D.; Yang, X. M.; Kim, T. K.; Nealey, P. F. *Langmuir* **2000**, *16*, 9620.
(23) Yang, X. M.; Peters, R. D.; Kim, T. K.; Nealey, P. F. *J. Vac. Sci. Technol. B* **1999**, *17*, 3203.
(24) Heier, J.; Kramer, E. J.; Walheim, S.; Krausch, G. *Macromolecules* **1997**, *30*, 6610.
(25) Heier, J.; Genzer, J.; Kramer, E. J.; Bates, F. S.; Walheim, S.; Krausch, G. *J. Chem. Phys.* **1999**, *111*, 11101.
(26) Heier, J.; Sivaniah, E.; Kramer, E. J. *Macromolecules* **1999**, *32*, 9007.
(27) Heier, J.; Kramer, E. J.; Groenewold, J.; Fredrickson, G. H. *Macromolecules* **2000**, *33*, 6060.
(28) Yang, X. M.; Peters, R. D.; Kim, T. K.; Nealey, P. F.; Brandow, S. L.; Chen, M.-S.; Shirey, L. M.; Dressick, W. J. *Langmuir* **2001**, *17*, 228.
(29) The interfacial energies reported in ref 17 were measured at room temperature, and therefore, the absolute values of γ in ref 17 are expected to be larger than the actual values at 180 °C. The behavior of interfacial energy with temperature is well-defined as discussed in ref 30 such that the relative values of γ and $\Delta\gamma$ at 25 and 180 °C are similar, and the same trends in $\Delta\gamma$ reported at 25 °C are expected at 180 °C.
(30) Fryer, D. S.; Peters, R. D.; Kim, E. J.; Tomaszewski, J. E.; de Pablo, J. J.; Nealey, P. F.; White, C. C.; Wu, W.-L. *Macromolecules* **2001**, in press.
(31) Yang, X. M.; Peters, R. D.; Nealey, P. F.; Solak, H. H.; Cerrina, F. *Macromolecules* **2000**, *33*, 9575.
(32) Coulon, G.; Collin, B.; Chatenay, D.; Gallot, Y. *J. Phys. II* **1993**, *3*, 697.
(33) Collin, B.; Chatenay, D.; Coulon, G.; Ausserre, D.; Gallot, Y. *Macromolecules* **1992**, *25*, 1621.
(34) Bassereau, P.; Brodbreck, D.; Russell, T. P.; Brown, H. R.; Shull, K. R. *Phys. Rev. Lett.* **1993**, *71*, 1716.
(35) Grim, P. C. M.; Nyrkova, I. A.; Semenov, A. N.; Tenbrinke, G.; Hadziioannou, G. *Macromolecules* **1995**, *28*, 7501.
(36) Ausserre, D.; Chatenay, D.; Coulon, G.; Collin, B. *J. Phys. Fr.* **1990**, *51*, 2571.
(37) Liu, Y.; Rafailovich, M. H.; Sokolov, J.; Schwarz, S. A.; Bahal, S. *Macromolecules* **1996**, *29*, 899.
(38) Smith, A. P.; Douglas, J. F.; Meredith, J. C.; Amis, E. J.; Karim, A. *Phys. Rev. Lett.* **2001**, in press.
(39) Russell, T. P.; Menelle, A.; Anastasiadis, S. H.; Satija, S. K.; Majkrzak, C. F. *Macromolecules* **1991**, *24*, 6263.
(40) Singh, N.; Kudrle, A.; Sikka, M.; Bates, F. S. *J. Phys. II Fr.* **1995**, *5*, 377.
(41) Ehlich, D.; Takenaka, M.; Hashimoto, T. *Macromolecules* **1993**, *26*, 492.
(42) Hamersky, M. W.; Tirrell, M.; Lodge, T. P. *J. Polym. Sci., Part B: Polym. Phys.* **1996**, *34*, 2899.
(43) Green, P. F.; Russell, T. P.; Jerome, R.; Granville, M. *Macromolecules* **1988**, *21*, 3266.

MA011003E